JOURNAL OF APPLIED ELECTROCHEMISTRY 24 (1994) 261–267

A boundary element method for transient diffusion

A. C. WEST

Columbia University, Department of Chemical Engineering, Materials Science, and Mining Engineering, New York, NY 10027, USA

M. MATLOSZ

Materials Department, Swiss Federal Institute of Technology, MX-C Ecublens, LMCH, CH-1015 Lausanne, Switzerland

Received 9 December 1992; revised 20 June 1993

Transient diffusion in two-dimensional geometries is considered. It is shown how the spatial variation of the mass transfer-limited flux of a minor species varies with time from initially uniform to the non-uniform, steady-state distribution. Flux distributions on sinusoidal electrode and on a line electrode embedded in an otherwise insulating plane are considered. A boundary-element method is used to solve the problem in Laplace transform space, and the results are subsequently inverted into the time domain.

List of symbols

$A_{i,j}$	fitting coefficients defined by Equation 15
c	dimensionless concentration
$\hat{c}$	dimensional concentration (mol cm^{-3})
c_∞	bulk concentration (mol cm^{-3})
D	diffusion coefficient (cm^2 s^{-1})
f	functions introduced in Equation 15
$\bar{f}$	Laplace transform of function introduced in Equation 15
g	Green's function for modified Helmholz equation
K_0, K_1	modified Bessel functions of the second kind of order zero and one
n_i	number of node points used in BEM calculation
N	number of values of s used in simulations
r	dimensionless distance, defined by Equation 8
s	Laplace transform variable, defined by Equation 5
q	dimensionless flux normal to the electrode
$\bar{q}$	Laplace transform of the dimensionless flux normal to the electrode
t	time (s)
x, y	dimensionless cartesian coordinates
$\hat{x}, \hat{y}$	dimensional cartesian coordinates (cm)
z	generic interpolation function

Greek symbols

α	geometric parameter
β_i	curve-fitting parameter used in exponential functions
ϵ_0	amplitude of sinusoidal roughness (cm)
Γ	boundary of computational domain
λ	wavelength of sinusoidal roughness (cm)
σ	dimensionless arc length
τ	dimensionless time
π	3.1415926...
ζ	path of integration

Subscripts

avg	average
max	maximum
min	minimum
q	point at which the concentration (or gradient) is determined
ss	steady-state

1. Introduction

Pulse electrolysis has been extensively investigated because it offers several advantages over steady-state processes [1–3]. Among these advantages is that the current distribution can be altered by adjusting the on and off times of the galvanic pulse. Some of these effects are discussed in [4–7]. Theoretical treatment of pulse plating may require the examination of transient, mass transfer-limited reaction rates of additives [8]. Mass transfer plays perhaps an even more crucial role in transient anodic processes [9, 10]. Other emerging technologies where transient mass transfer phenomena are important include analytical microelectrode applications [11, 27], where high potential sweep rates are achieved during voltammetry [12], and mass-transfer sensors [13] for studying hydrodynamic fluctuations.

The primary goal of this paper is to demonstrate transient mass transfer effects. The second objective is to discuss a solution procedure for solving the two-dimensional, transient-diffusion equation:

$$\frac{\partial \hat{c}}{\partial t} = D\left(\frac{\partial^2 \hat{c}}{\partial \hat{x}^2} + \frac{\partial^2 \hat{c}}{\partial \hat{y}^2}\right) \quad (1)$$

A boundary-element method for finding numerical

0021-891X

solutions to Equation 1 in Laplace transform space is used. The solutions are subsequently inverted into the time domain. Such a solution procedure has been discussed by Ligget and Liu [14] and Brebbia *et al.* [15], but has not been used previously in electrochemical systems.

The efficacy of the numerical method is evaluated for the two geometries shown in Figs 1 and 2. The geometry of Fig. 1 might represent sinusoidal roughness on an electrode and is often used for model studies of anodic levelling [16–18]. The second problem (Fig. 2) corresponds to a two-dimensional line electrode embedded in a coplanar insulating plane. The steady-state current distribution on this electrode has been given by Wagner [19]. Diem *et al.* [20] treated the finite-domain cell. Due to the singularity at the electrode edge, this problem is a particularly challenging test of the numerical method.

2. Theory

Equation 1 can be made more tractable by introducing the dimensionless variables:

$$x = \frac{\hat{x}}{L}; \quad y = \frac{\hat{y}}{L}; \quad c = \frac{c_\infty - \hat{c}}{c_\infty}; \quad \tau = \frac{Dt}{L^2} \tag{2}$$

where L is a characteristic length and c_∞ is the bulk concentration. Substitution of these definitions into Equation 1 gives

$$\frac{\partial c}{\partial \tau} = \frac{\partial^2 c}{\partial x^2} + \frac{\partial^2 c}{\partial y^2} \tag{3}$$

The application of the Laplace transform method to partial differential equations is found in many standard texts [21]. Equation 3 becomes

$$s\bar{c} - c_{\tau=0} = \frac{\partial^2 \bar{c}}{\partial x^2} + \frac{\partial^2 \bar{c}}{\partial y^2} \tag{4}$$

where $c_{\tau=0}$ is the dimensionless concentration at zero time, and

$$\bar{c}(x, y; s) = \mathscr{L}\{c\} = \int_0^\infty e^{-s\tau} c(x, y, \tau)\, d\tau \tag{5}$$

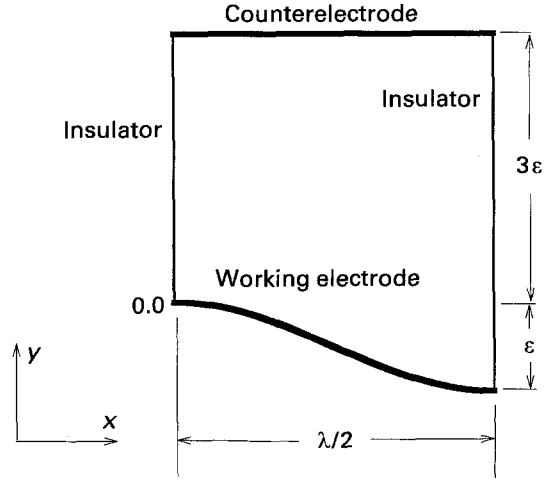

Fig. 1. Schematic of the computational domain used to simulate transient, mass transfer-limited flux distributions on a sinusoidal electrode.

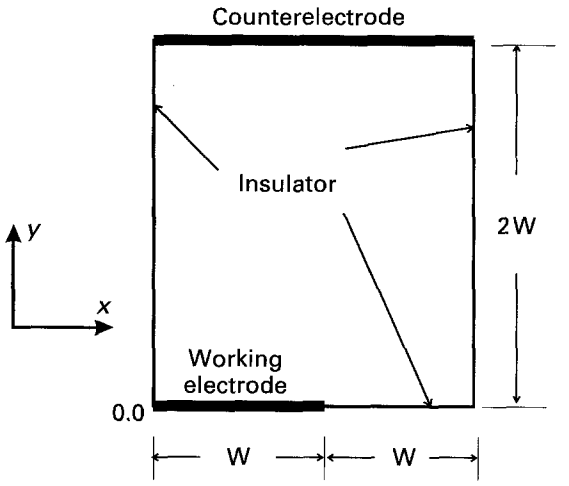

Fig. 2. Geometry used to simulate mass transfer distributions on a two-dimensional line electrode.

Equation 4 is sometimes known as the modified Helmholtz equation [21]. The boundary conditions would be transformed in the same manner.

2.1. *Boundary integral equations*

The use of Green's functions for solving partial differential equations is described, for example, by Greenberg [22]. It can be shown that Equation 4 can be reformulated as an integral equation:

$$\alpha \bar{c}(x_q, y_q; s) = \int_\Gamma \left(g(x, y; s) \frac{\partial \bar{c}(x, y; s)}{\partial n} - \bar{c}(x, y; s) \frac{\partial g(x, y; s)}{\partial n} \right) d\zeta + \iint_A c_{\tau=0}(x, y) g(x, y; s)\, dx\, dy \tag{6}$$

where $\alpha = 1$ if the point x_q, y_q is inside the domain, $\alpha = 0$ when the point is outside the domain, and $\alpha = 1/2$ if the point is on a locally smooth boundary. The first integral on the right side of Equation 6 is a line integral along the closed path ζ, which is taken to be in the counterclockwise direction around the simply connected boundary Γ. The second is an area integral over the computational domain. The integrand depends on the known initial conditions; thus, the integral must only be evaluated once for each point x_q, y_q.

The Green's function g is given by [14]

$$g(x, y; s) = \frac{1}{4\pi} K_0(r\sqrt{s}) \tag{7}$$

where K_0 is the modified Bessel function of the second kind of order zero, and

$$r = [(x - x_q)^2 + (y - y_q)^2]^{1/2} \tag{8}$$

The normal component of the gradient of the Green's function is given by

$$\frac{\partial g}{\partial n} = -\frac{\sqrt{s}}{4\pi} K_1(r\sqrt{s}) \frac{\partial r}{\partial n} \tag{9}$$

where K_1 is the modified Bessel function of the second

kind of order one. Polynomial approximations of K_0 and K_1 can be found in Abramowitz and Stegun [23]. Equations 6–9 are solved for values of s that are chosen to facilitate the inversion of the results from Laplace space into the time domain.

The boundary conditions that are assumed in this study are

$$\left.\begin{aligned} &\partial c/\partial n = 0 \text{ along all insulators} \\ &c = 0 \text{ at the counterelectrode for all times} \\ &c = 1 \text{ at the working electrode for all } \tau > 0 \end{aligned}\right\} \tag{10}$$

and the initial condition is

$$c = 0 \text{ at } \tau = 0 \text{ for all } x \text{ and } y \tag{11}$$

In Laplace transform space, the condition along the working electrode becomes

$$\bar{c} = 1/s \tag{12}$$

and the homogeneous boundary conditions for $\bar{c}$ are the same as the conditions on c.

3. Numerical method

3.1. *Boundary-element method*

With initial condition 11 ($c_{\tau=0} = 0$), Equation 6 for points x_q, y_q outside of the domain ($\alpha = 0$) takes on the following form:

$$\int_\Gamma \left(\bar{c}(x,y;s)\frac{\partial g(x,y;s)}{\partial n}\right) d\zeta = \int_\Gamma \left(g(x,y;s)\frac{\partial \bar{c}(x,y;s)}{\partial n}\right) d\zeta \tag{13}$$

Equation 13 is identical to the integral equations used for previous calculations of current distributions [24]. As a result, the same algorithms may be employed simply by replacing the Green's function and its normal derivative with those given in Equations 7 and 9. The boundary-element formulation suggested by Equation 13, where the nodal points x_q, y_q are outside the domain instead of on the boundary, has been discussed previously by Walker [25].

For numerical solution, at a given value of s, the boundary of the domain is discretized into n_j linear two-point elements, numbered sequentially in the counterclockwise direction around the domain boundary. Boundary coordinates, transformed boundary concentrations and concentration derivatives along an element j are then given by the following linear interpolation expression:

$$z_j = \frac{1-\sigma}{2} z_{1,j} + \frac{1+\sigma}{2} z_{2,j} \tag{14}$$

where

$z = x$ for x-coordinates
$z = y$ for y-coordinates
$z = \bar{c}$ for transformed concentrations
$z = \dfrac{\partial \bar{c}}{\partial n}$ for normal concentration derivatives

with indices 1 and 2 denoting respectively the tail and head of the element. The variable σ, where $-1 \leqslant \sigma \leqslant 1$, represents a dimensionless arc length along an element from the tail ($\sigma = -1$) to the head ($\sigma = 1$). In the present study, higher-order interpolation functions were not considered.

As in previous studies [24, 31, 32], boundary points are shared for adjacent elements when the same boundary conditions are imposed, but are doubled when the conditions are different (i.e. the same geometrical coordinates at the intersection of two elements correspond to two distinct node points, each subject to the boundary condition imposed on one of the adjacent elements). Depending on the number of elements and on the number of doubled points, the discretization procedure results in a number of distinct node points n_i where $n_i > n_j$. Alternative discretization procedures to node-point doubling at the electrode/insulator edges were not considered.

Depending on the boundary conditions, at each independent node i either the transformed concentration $\bar{c}$ or the transformed normal gradient $\partial\bar{c}/\partial n$ of the concentration is known. Hence for n_i node points, n_i independent equations in the form of Equation 13 are necessary. Each equation represents an integral over the entire boundary using the Green's function $g_q(x,y;s)$ associated with the point x_q, y_q. Following the discretization procedure, each Equation 13 may be written as a sum of nodal unknowns multiplied by appropriate integrals over the element lengths. The resulting set of equations can be solved by conventional matrix methods (we used Gauss–Jordan elimination with full pivoting).

For the matrix procedures to be effective numerically, the points x_q, y_q for each Equation 13 are chosen to be near one of the node points on the boundary. The resulting matrix equations are then diagonally dominant, which facilitates their inversion. If the points are too close to the boundary, however, numerical difficulties resulting from the singularities in the Green's function may occur. Consequently, a compromise in the selection of the positions is necessary, and the suggestion of Walker [25] has been adopted here (points x_q, y_q are generally chosen to be located outside of the domain a normal distance from a given nodal point equal to the average length of the two elements intersecting at that node.) For doubled points, special attention must be given to avoid two x_q, y_q at the same position.

For all results reported in this study, boundary nodes were placed to assure a nearly uniform element length everywhere on the boundary. The element length was set by dividing the working electrode into 80 elements. Doubling the number of elements did not change appreciably the simulation results. Gaussian quadrature was employed for numerical integration. It was found that 12-point and 24-point formulae give essentially identical results; hence, the 12-point formulae were employed for the results shown below.

3.2. *Inversion of Laplace transforms*

If Laplace-space solutions are found for N values of s, time-domain answers can be determined by a series expansion of N assumed functions of time with known Laplace transforms [14, 28]. The inversion is achieved by expanding the concentration gradient at *each* point j as a series of N known time functions:

$$q_j - q_{j,\mathrm{ss}} = \sum_{i=1}^{N} A_{i,j} f_i(\tau) \tag{15}$$

where

$$q = \frac{\partial c}{\partial n} \tag{16}$$

The Laplace transform of Equation 15 evaluated at $s = s_k$ can be expressed as

$$\bar{q}_j(s_k) - \frac{q_{j,\mathrm{ss}}}{s_k} = \sum_{i=1}^{N} A_{i,j} \bar{f}_i(s_k) \tag{17}$$

Since N values of $\bar{q}_j(s_k)$ are known, the unknown coefficients $A_{i,j}$ can be evaluated by inverting an $N \times N$ matrix. The procedure is repeated for all points j.

The functions $f_i(\tau)$ must have known Laplace transforms and are generally chosen by recognizing the features of the expected solution. The functions used here to predict the flux distribution in response to a step change in the surface concentration are

$$f_i(\tau) = \exp(-\beta_i \tau) \tag{18}$$

The corresponding Laplace-space functions are

$$\bar{f}_i(s) = \frac{1}{\beta_i + s} \tag{19}$$

The N constants β_i were arbitrarily set equal to the N values of s_i used in the calculations. Consequently, Equation 17 becomes

$$\bar{q}_j(s_k) - \frac{q_{j,\mathrm{ss}}}{s_k} = \sum_{i=1}^{N} \frac{A_{i,j}}{s_i + s_k} \tag{20}$$

To accomplish the inversion into the time domain, it is recommended that the N values of s be chosen according to

$$s_k = s_{\min} \left(\frac{s_{\max}}{s_{\min}} \right)^{(k-1)/(N-1)} \tag{21}$$

where $s_{\min}$ and $s_{\max}$ are the minimum and maximum values of s. For both problems studied here, the following parameters were used: $s_{\min} = 0.001$, $s_{\max} = 1000$, and $N = 13$. It was found that increasing or decreasing $s_{\min}$ and $s_{\max}$ by an order of magnitude did not significantly change the time-domain results. Likewise, results did not change significantly for $10 \leqslant N \leqslant 16$.

4. Sinusoidal electrode

Figure 1 shows the cell geometry used to study a sinusoidal electrode. The counterelectrode is assumed to be placed at a distance 3ϵ from the maximum height of the working electrode. Clerc and Landolt [18] show that the steady-state flux distribution is unchanged by placing the counterelectrode at further distances from the working electrode. Consequently, the influence of the counterelectrode must also be negligible during a transient. For this geometry, the characteristic length was chosen to be $L = \lambda/2$.

Results are given for three amplitude-to-wavelength ratios. Figure 3 shows the steady-state, diffusion-limited flux variations for these three ratios. The solutions were obtained by a boundary-element method for Laplace's equation [24]. The spatial variation increases as the dimensionless amplitude increases.

Figure 4 shows the spatial variation of the dimensionless Laplace-space fluxes for various values of s for $\epsilon/\lambda = 0.25$. As $s \to \infty$, corresponding to $\tau \to 0$, the distribution of the mass transfer rate becomes uniform. This is expected since the diffusion-layer thickness is initially infinitesimally small and follows exactly the surface contour.

Figures 5, 6 and 7 show the variation in the time domain for various dimensionless times. For comparison, the steady-state solution (dotted line) is shown. It can be seen that the spatial variation of the normal flux near the electrode edges is in accord with what should be expected for a 90 degree angle of intersection between the electrode and insulators [30]; i.e. the first derivative of the flux distribution at the electrode edge is zero. Roughly speaking, for all dimensionless times $\tau > 1$, the steady-state variation of the flux is valid, and for all $\tau < 10^{-3}$, the distribution is nearly uniform. It is seen that the time required to reach steady state increases with the dimensionless amplitude.

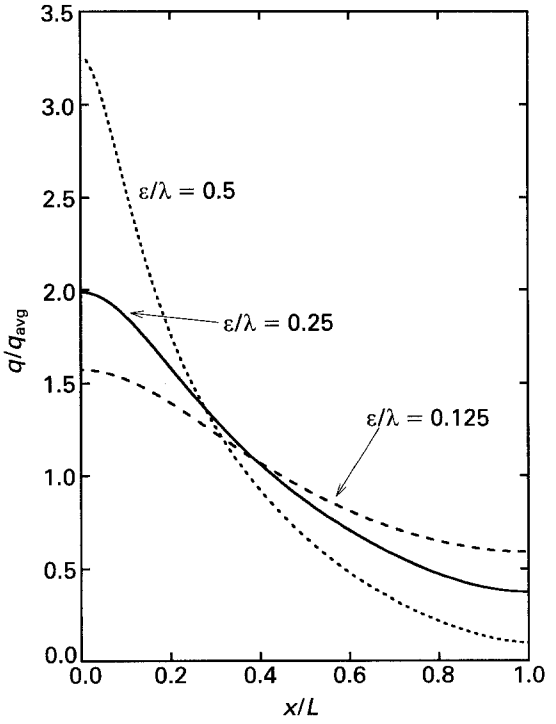

Fig. 3. Steady-state flux distribution on sinusoidal electrode for three amplitude/wavelength ratios.

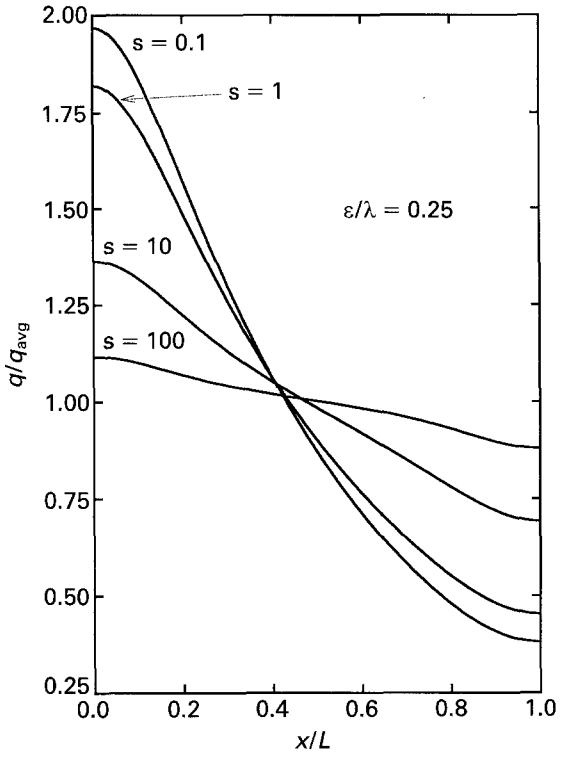

Fig. 4. Normalized s-domain flux distributions for an amplitude/wavelength ratio of 0.25.

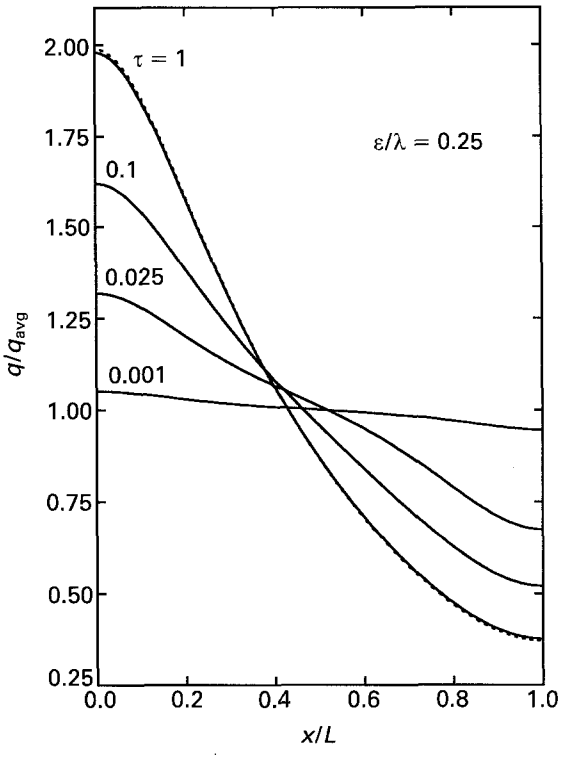

Fig. 6. Normalized flux distributions at four times for $\epsilon/\lambda = 0.25$. The steady-state distribution (dashed line) is shown for comparison.

5. Two-dimensional line electrode

A two-dimensional line electrode embedded in an insulating plane is shown in Fig. 2. To avoid numerical complications, a finite domain is assumed. The side insulating wall is placed at $x = 2W$, and the counterelectrode is at $y = 2W$. The steady-state flux distribution of the finite-domain geometry is nearly indistinguishable from that of the semi-infinite domain. For the results reported below, $L = W$.

Figure 8 shows Laplace-space flux distributions for four values of s. Again, the nonuniformity increases as s decreases. Near $x/L = 1$, irregularities in the numerically calculated flux distribution are observed. Increasing the node density decreases the

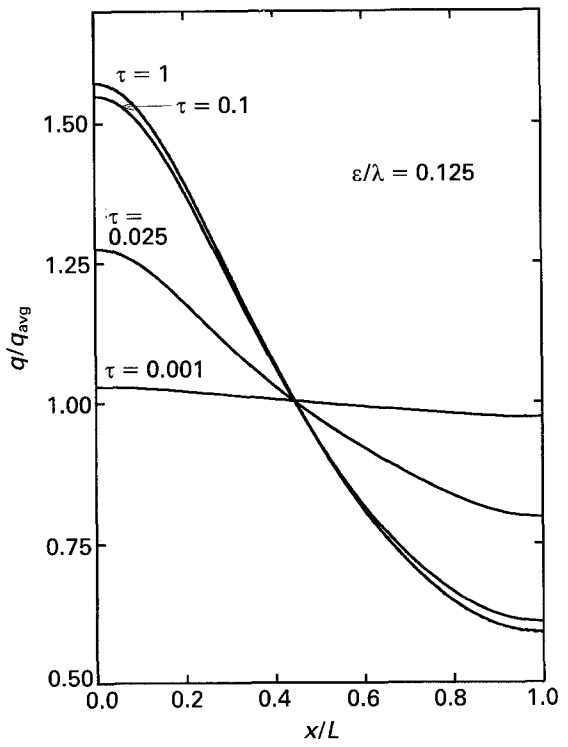

Fig. 5. Normalized flux distributions at four times for $\epsilon/\lambda = 0.125$. The steady-state distribution is indistinguishable from the distribution at $\tau = 1$.

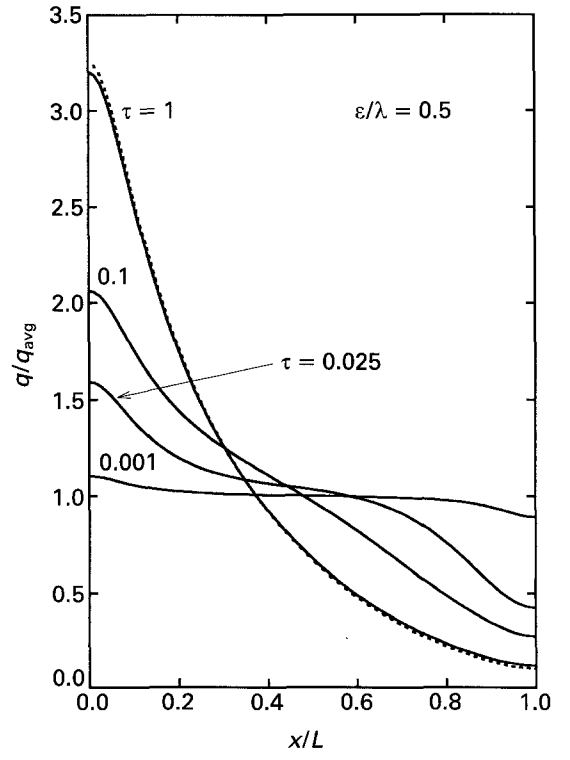

Fig. 7. Normalized flux distributions at four times for $\epsilon/\lambda = 0.5$. The steady-state distribution (dashed line) is shown for comparison.

distance from the electrode edge where such irregularities occur. Nevertheless, without using special interpolation functions near the singular points, it is quite difficult to eliminate the irregularities completely. This is a well known problem when boundary-element methods are used for Laplace's equation. The problem may be especially noticeable when the angle of intersection between the electrode and insulator is obtuse. Experience has shown that the errors often do not propagate throughout the computational domain [29].

Figure 9 shows flux distributions for various dimensionless times. For $\tau > 1$, the flux distribution is nearly identical to the steady-state distribution (dashed line). For $\tau < 10^{-3}$, the distribution is practically uniform except for a small region near $x = L$. Resolution of the flux distribution near this edge would require a singular-perturbation analysis, which is beyond the scope of this work. The non-smooth behaviour in the edge region results from the irregular Laplace-space solutions obtained from the boundary-element method.

In addition to the normalized flux distribution, knowledge of the variation of the average flux with time may be interesting. Figure 10 shows the simulated temporal variation of the average flux normalized by the steady-state, average flux. For comparison, the dashed line gives the asymptotic short-time behaviour:

$$q_{\text{avg}}(\tau \to 0) = \frac{1}{\sqrt{(\pi\tau)}} \tag{23}$$

The asymptotic solution is approached for $\tau < 0.05$. The kink in the curve near $\tau = 0.07$ is a numerical artifact, associated with the inherent difficulties in performing numerically an inverse Laplace transform.

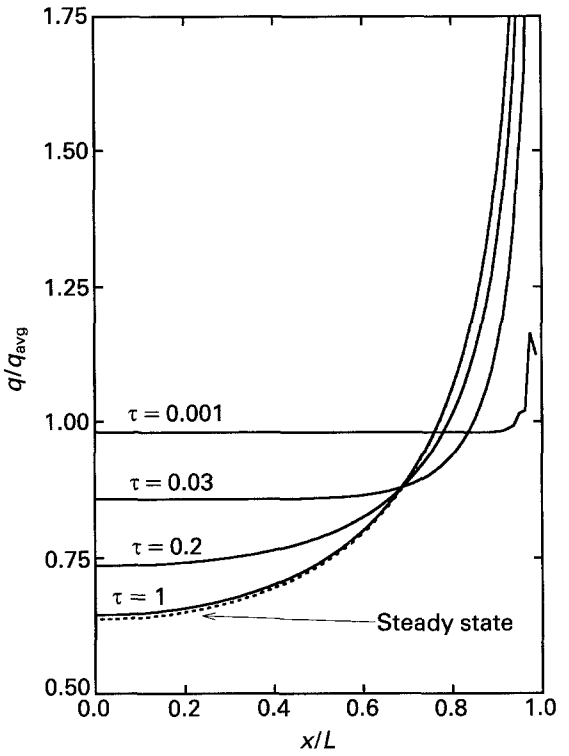

Fig. 9. Normalized flux distributions on a two-dimensional line electrode at four times. The steady-state distribution (dashed line) is shown for comparison.

6. Discussion of numerical method

One objective of this paper is to present a numerical method for solving the two-dimensional,

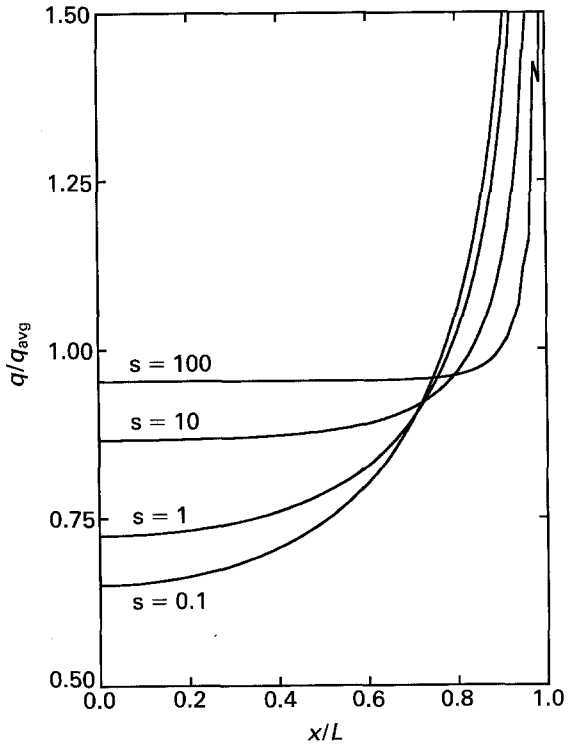

Fig. 8. Normalized s-domain flux distributions on a two-dimensional line electrode for four values of s.

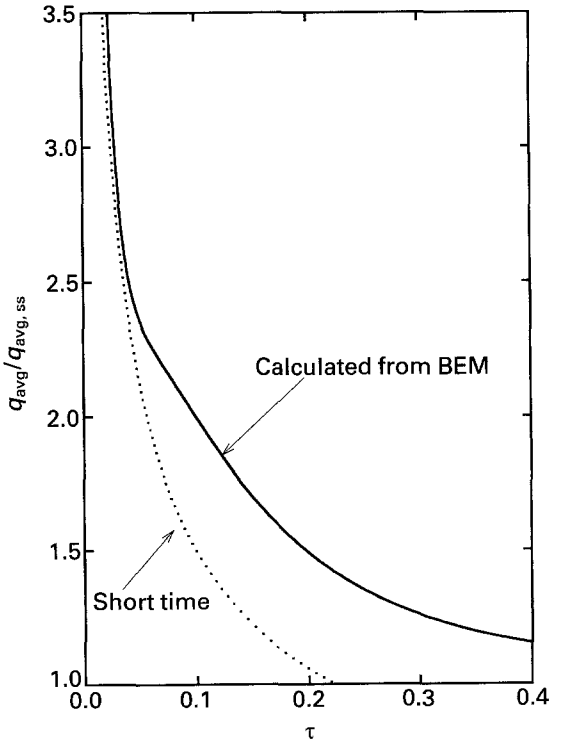

Fig. 10. The average flux, normalized by the steady-state average flux, as a function of time as predicted by the BEM simulations and the asymptotic solution valid at short times.

transient-diffusion equation. Two issues are involved in the evaluation of the numerical technique. The first is whether boundary-element code, in which many electrochemists have invested a significant amount of time, can be easily extended to investigate other phenomena governed by linear operators. The second issue concerns the effectiveness of the Laplace transform approach to handling transient-diffusion problems.

The development of a numerical method can be tedious because it is often necessary to search for optimal parameter settings that cannot be *a priori* chosen. Such an optimization was performed for the steady-state, two-dimensional diffusion operator. It was subsequently discovered that the same settings are adequate for the axisymmetric operator, which has a different Green's function. Here, a third Green's function was tested. We again found that it was not necessary to vary parameter settings. These are promising observations because they suggest that boundary-element code optimized for the Laplace operator can be easily upgraded into code for a large number of linear differential operators with known Green's functions.

The second point of this paper is to explore one possible way of solving Equation 1. Brebbia *et al.* [15] and Pina and Hernandes [26] discuss an alternative formulation using a boundary-element method. The alternative procedure approximates the time derivative in Equation 1 by a finite-difference equation and involves solving the boundary-integral equations at successive timesteps. They suggest that this procedure is more general, and would be especially useful when the boundary conditions are complicated functions of time. The Laplace transform method is potentially more efficient, but inversion back into the time domain can be difficult. Consequently, since the cost of computation continues to decrease, we also recommend the more robust method.

7. Summary

Boundary-element methods designed for solving Laplace's equation can be extended to solve the modified Helmholtz equation. Results of these simulations correspond to solving the two-dimensional, transient-diffusion equation in Laplace transform space. For the two cell geometries investigated here, fitting the numerical results to a series of functions with known inverse Laplace transforms successfully yielded time-domain solutions.

The mass transfer distribution in response to a step change in surface concentration is initially uniform. For a two-dimensional line electrode embedded in a coplanar insulating plane, the flux distribution is roughly given by the steady-state distribution for all dimensionless times $\tau > 1$. The mass transfer distribution to a sinusoidal electrode was also considered. For the cases studied, the dimensionless time necessary to approach steady state was also found to be of the order of one, increasing slightly with the amplitude/wavelength ratio.

References

[1] N. Ibl, *Surf. Technol.* **10** (1980) 81.
[2] J.-C. Puippe and F. Leaman (eds), 'Theory and Practice of Pulse Plating', American Electroplaters and Surface Finishers Society, Orlando, FA (1990).
[3] A. M. Pesco and H. Y. Cheh, *J. Electrochem. Soc.* **136** (1989) 408.
[4] D.-T. Chin, N. R. K. Vilambi and M. K. Sunkara, *Plat. Surf. Finish.* **76** (Oct. 1989) 74.
[5] H. H. Wan and H. Y. Cheh, *J. Electrochem. Soc.* **135** (1988) 658.
[6] *Idem ibid.* **135** (1988) 643.
[7] P. S. Fedkiw and D. R. Brouns, *ibid.* **135** (1988) 346.
[8] K. G. Jordan and C. W. Tobias, *ibid.* **138** (1991) 1251.
[9] K. G. Jordan and C. W. Tobias, *ibid.* **138** (1991) 3581.
[10] D. Landolt, *Electrochim. Acta* **32** (1987) 1.
[11] D. R. Baker, M. W. Verbrugge and J. Newman, *J. Electroanal. Chem.* **314** (1991) 23.
[12] R. M. Wightman, *Science* **240** (1988) 415.
[13] T. J. Hanratty, *J. App. Electrochem.* **21** (1991) 1038.
[14] J. A. Liggett and P. L.-F. Liu, 'The Boundary Integral Equation Method for Porous Media Flow', Allen and Unwin, Boston (1983).
[15] C. A. Brebbia, J. C. F. Telles and L. C. Wrobel, 'Boundary Element Techniques, Theory and Applications in Engineering', Springer-Verlag, Berlin (1984).
[16] C. Wagner, *J. Electrochem. Soc.* **101** (1954) 225.
[17] P. S. Fedkiw, *J. Electrochem. Soc.* **127** (1980) 1304.
[18] C. Clerc and D. Landolt, *Electrochim. Acta* **29** (1984) 787.
[19] C. Wagner, *J. Electrochem. Soc.* **98** (1951) 116.
[20] C. B. Diem, B. Newman and M. E. Orazem, *J. Electrochem. Soc.* **133** (1988) 2524.
[21] F. B. Hildebrand, 'Advanced Calculus for Applications', (2nd edn), Prentice-Hall, Englewood Cliffs, NJ (1976).
[22] M. D. Greenberg, 'Application of Green's Functions in Science and Engineering', Prentice-Hall, Englewood Cliffs, NJ (1971).
[23] M. Abramowitz and I. A. Stegun, 'Handbook of Mathematical Functions', Dover, New York (1964) Equations 9.8.5–9.8.8, p. 379.
[24] M. Matlosz, C. Creton, C. Clerc and D. Landolt, *J. Electrochem. Soc.* **134** (1987) 3015.
[25] S. Walker, *in* 'Boundary Element Methods', (edited by C. A. Brebbia), Third International Seminar, Irvine, CA, July 1981, Springer Verlag, Heidelberg (1981) p. 472.
[26] H. L. G. Pina and J. L. M. Fernandes, 'Applications in Transient Heat Conduction', *in* 'Topics in Boundary Element Research', Vol. 1, (edited by C. A. Brebbia), Springer-Verlag, Berlin (1984).
[27] M. V. Mirkin and A. J. Bard, *J. Electroanal. Chem.* **323** (1992) 1.
[28] F. J. Rizzo and D. J. Shippey, *AIAA J.* **8** (1970) 2004.
[29] A. C. West, C. Madore, M. Matlosz and D. Landolt, *J. Electrochem. Soc.* **139** (1992) 499.
[30] A. C. West and J. Newman, 'Determining Current Distributions Governed by Laplace's Equation', *in* 'Modern Aspects of Electrochemistry, No. 23, (edited by B. E. Conway *et al.*), Plenum Press, New York (1992).
[31] C. Brebbia, 'The Boundary Element Method for Engineers', John Wiley & Sons, New York (1978).
[32] J. Deconinck, Dissertation, Vrije Universiteit Brussel, Brussels, Belgium (1985).